Mühendis ve Makina / Engineer and Machinery
https://dergipark.org.tr/tr/pub/muhendismakina

OPTIMIZATION OF A THERMOELECTRIC COOLER FOR A TURBOCHARGED TRACTOR

Ali Kürşad ARICIOĞLU[1], Gülay YAKAR[2*], Ali GÜRCAN[3]

[1] Akdeniz Üniversitesi, Mühendislik Fakültesi, Makine Mühendisliği Bölümü, Antalya
ORCID No : http://orcid.org/0000-0001-6293-4237

[2] Pamukkale Üniversitesi, Mühendislik Fakültesi, Makine Mühendisliği Bölümü, Denizli
ORCID No : http://orcid.org/0000-0002-1865-7815

[3] İstanbul Gelişim Üniversitesi, İstanbul Gelişim Meslek Yüksekokulu, Makine Bölümü, İstanbul, ORCID No : http://orcid.org/0000-0002-2745-1413

Keywords

Thermoelectric, cooler, electric, power input

Abstract

This work covers a numerical analysis of the design and optimization of a thermoelectric cooler (TEC) operated by a thermoelectric generator (TEG). The aim of the work was to design the optimum mini refrigerator for tractors and also to provide cooling using the energy produced in the TEG used in the tractor. Thanks to the TEC powered with the TEG system, farmers will be able to preserve their food during working hours without additional fuel consumption. When the literature is examined, no study has been found in which cooling is done by using the compressor air of turbocharged systems. Therefore, this work will make an important contribution to the literature. According to the numerical results obtained, while the electrical power requirement was 34.78 W at an outdoor temperature of 30 °C, it was 26.54 W at an outdoor temperature of 15 °C. In other words, while the coefficient of performance was obtained as 0.301 at 15 °C, it was determined as 0.219 at 30 °C. In addition, while the electrical power value produced by the TEG system used in the tractor for an outdoor temperature of 15 °C was 50.71 W, it was 38.84 W at an outdoor temperature of 30 °C.

* gyakar@pau.edu.tr
doi : 10.46399/muhendismakina.1427599

TURBOŞARJLI BİR TRAKTÖR İÇİN BİR TERMOELEKTRİK SOĞUTUCUNUN OPTİMİZASYONU

Anahtar Kelimeler

Termoelektrik, soğutucu, elektrik, güç girişi

Öz

Bu çalışma, bir termoelektrik jeneratör (TEJ) tarafından çalıştırılan bir termoelektrik soğutucunun (TES) tasarımı ve optimizasyonunun sayısal bir analizini kapsamaktadır. Çalışmada, traktörler için optimum mini buzdolabının dizayn edilmesi ve aynı zamanda traktörde kullanılan TEJ'de üretilen enerji ile soğutmanın sağlanması amaçlandı. TEJ sistemi ile çalıştırılan TES sayesinde çiftçiler, ek yakıt tüketimine gerek kalmadan, mesai saatleri içerisinde gıdalarını muhafaza edebilecekler. Literatür incelendiğinde, turboşarjlı sistemlerin kompresör havası kullanılarak soğutmanın yapıldığı herhangi bir çalışmaya rastlanmamıştır. Dolayısıyla bu çalışma, literatüre önemli bir katkı sağlayacaktır. Elde edilen sayısal sonuçlara göre, elektrik gücü ihtiyacı 30 °C dış sıcaklıkta 34,78 W iken, 15 °C dış sıcaklıkta 26,54 W olarak elde edilmiştir. Yani performans katsayısı 15 °C'de 0,301 olarak elde edilirken, 30 °C'de 0,219 olarak belirlendi. Ayrıca traktörde kullanılan TEJ sisteminin, 15 °C dış ortam sıcaklığında ürettiği elektrik gücü değeri 50,71 W iken, 30 °C dış ortam sıcaklığında 38,84 W olmuştur.

Araştırma Makalesi
Başvuru Tarihi : 29.01.2024
Kabul Tarihi : 15.03.2024

Research Article
Submission Date : 29.01.2024
Accepted Date : 15.03.2024

1. Introduction

Today, advances in technology and a growing interest in comfort conditions mean that the need for proper cooling is increasing daily. Systems that use thermoelectric (TE) modules are widely employed for the purposes of heating, cooling and generating electricity. Such systems are simple and relatively maintenance-free. If they are used to generate electricity, they are given the name TEGs, while they are referred to as TECs when used for cooling. Cheng and Lin (2005) emphasized that both the coefficient of performance and the cooling capacity of TEC modules are highly important. They suggested a method to optimize the dimensions of the TEC legs using genetic algorithms, in order to maximize the cooling capacity. Their results showed that optimizing the dimensions of the TEC module can enhance the cooling capacity. Khattab and El Shenawy (2006) conducted a study on the optimal operating conditions of a small TEC driven by a solar TEG. They determined that five thermocouples of the TEG could drive one thermocouple of the TEC. In other words, their results indicated that 10 TEG modules would be needed to operate the TEC used at optimum performance for most of the year.

Meng, Chen and Sun (2010) used non-equilibrium thermodynamic theory to analyze the extreme operating temperature difference of a combined TE system consisting of a TEC or a heat pump driven by a TEG. Their results indicated that a 60 K temperature difference for cooling or 200 K for heating can be obtained if a TEG actuates under a temperature difference of 150 K. Chen, Meng and Sun (2012) suggested a TE refrigerator model with external heat transfer driven by a TEG. They investigated the effects of the allocation of the thermoelement and heat transfer area using numerical examples that were highly detailed. They were able to obtain an optimum operating electric current with regard to the maximum cooling load and coefficient of performance, with different total numbers of thermoelements and a different total heat transfer area. Chen, Wang and Hung (2014) numerically analyzed a geometrically designed integrated TEG-cooling system by means of a finite element technique. The maximum reduction percentages of system performance that they obtained were 12.45% and 18.67%, when the TEG and TEC lengths were altered. Attar, Lee and Weera (2015) experimentally validated the optimum design required for an automotive air-to-air TE air conditioner. The optimum design of the TE air conditioner was obtained with a new method using the recently developed dimensional analysis. Hasani and Rahbar (2015) experimentally studied the recovery of TE waste heat from a PEM fuel cell. Their results indicated that the use of TECs was a viable method for the recovery of such heat from a PEM fuel cell. In addition, the overall efficiency of the system decreased as the leaving water temperature increased.

Manikandan and Kaushik (2015) proposed and analyzed a combined system

using the technique of maximum power point tracking in order to achieve the greatest possible cooling power alongside overall efficiency. They demonstrated the impact of the source temperature of the TEG and TEC, and the heat transfer area on how the combined system performed. Their results found that the external irreversibilities reduced cooling power of the combined system and the overall efficiency by 36.49% and 16.9%, respectively. Zhang, Kong, Dong, Xu, Chen and Ni (2017) proposed an innovative hybrid system consisting primarily of a TEG, a TEC and solid oxide fuel cells used in the recovery of waste heat from the latter for in order to enhance performance. Their work took full account of the thermodynamic and electrochemical irreversible losses from every specific component. They also detailed the equivalent power output and efficiency for the hybrid system under differently operating regions of current density. They found that the power density and efficiency of the system proposed were 2.3% and 4.6% larger respectively than those of the stand-alone solid oxide fuel cells. Feng, Chen, Meng and Sun (2018) established a thermodynamic model for a TEC powered by a TEG device, taking into account the Thomson effect, analyzing and optimizing its performance. Their conclusions indicated that the Thomson effect reduced the productivity of the TEC-TEG, in that it decreased the cooling capacity by 27 %, as well as decreasing the coefficient of performance by 19 %.

Nemati, Nami, Yari and Ranjbar (2018) carried out exergy and exergoeconomic analyses of an electrically separated two-stage TEC. They found that the optimal first-stage current was lower than that of second-stage current, and, in addition, that the maximum exergy efficiency was obtained with currents at lower values compared to the minimum cooling cost. Lin, Zhang, Liu, Meng, Chen and Wang (2019) improved and extensively investigated single-stage and two-stage TEC-TEG systems. They proposed a fresh design for combined TEC-TEG systems using two single-stage TEGs to power the hot stage and the cold stage of the TEC separately. They found that the new design both increased the system's cooling capacity and increased the maximum temperature drop in the TEC. Kishore, Nozariasbmarz, Poudel, Sanghadasa and Priya (2019) studied in combination the effect of heat sink thermal resistances and TE material properties on TEC performance. Their results showed that efficient TECs are able to bring human skin down to a temperature 8.2 °C beneath the ambient temperature. That is, their modules achieved a 70% higher cooling than commercial modules. Sun, Liu, Shen, Chen, Yao and Jin (2019) intended to construct a model high-power light-emitting diode package integrated with a micro-TEC and to examine its performance with regard to several different interfacial and size effects. They determined that the best cooling performance was found in a micro-TEC with 6×6 TE elements for the driving power of a micro-TEC that was less than 0.85 W.

Sadighi Dizaji, Jafarmadar, Khalilarya and Pourhedayat (2019) experimentally

examined the impact of a number of parameters on exergy destruction and the performance of the second law through a TE air cooler. Their study explained the consequences of flow and thermodynamic parameters, among them DC voltage/ampere, incoming water temperature, water flow rate, incoming air temperature, and air flow rate on exergetic characteristics. They obtained a critical DC voltage value where the second law performance obtained minimum/maximum values. Lu, Li, Zhang, Ning and Niu (2020) built a three-dimensional trapezoidal TEC model at full scale in order to test its mechanical reliability and cooling performance through finite element simulation. Their results function as a helpful guide for designing trapezoidal TECs. Gonzalez-Hernandez (2020) studied the energetic analysis of a TEC, with optimization criteria being unified through the "x" variable. He suggested new modes of operation for both cooler and heater. Shen, Zhang, Liu, Tu, Lu, Chen and Huang (2020) proposed a segmented TEC for the purpose of enhancing cooling performance while not increasing the overall figure of merit. They developed the governing equations and physical model of the segmented TE element with regard to internal heat distribution and transport. Their results indicated that the segment number had a higher sensitivity to the thermal conductivity of the TE material, while the temperature difference and maximum cooling capacity of the segmented TE element were greater than those the conventional TE element.

Tian, Asaadi, Moria, Kaood, Pourhedayat and Jermsittiparsert (2020) examined the geometric characteristics of a tubular TEC as an air cooler, which have not been reported before. They found that a tubular TEC can be used for the purpose in question if the thermal and geometric parameters chosen are within the desired range. Qiu and Shi (2020) constructed a model with the aim of determining the factors influencing the cooling capacity of a TEC qualitatively and quantitatively utilizing finite element analysis. Their results indicated that there was a 35.73% and 21.59% improvement in the cooling capacity and the coefficient of performance of an optimized TEC with a non-constant cross-section, respectively, in comparison to a constant cross-section TEC. Kwan, Gao, Zhao, Ren, Hu, Dabwan and Pei (2021) analyzed whether it was feasible to integrate the radiative sky cooling capability of common photovoltaic cells into the photovoltaic-TEC in order to increase the space cooling energy density to a further extent. Huang, Chen and Ding (2021) examined a new two-stage TEC in a configuration that was electrically parallel. They detected that the thermocouple ratio between the two stages, the area-to-length ratio of the legs, and the cold side temperature had a significant impact on some important performance characteristics. Chen, Shi, Zou and Chen (2022) comprehensively reviewed the progress of cutting-edge on-chip TECs and outlined the relevant fundamentals, materials, designs, and system logic.

Sun, Shen, Niu, Gao, Zhou, Tang … Yang (2022) developed a numerical model with three dimensions in order to explore the micro-TEC's potential to reduce the negative impact of the fluctuating hot spot arising from thermal shock. Their results showed that the micro-TEC was able to check the temperature fluctuation seen in the chip subjected to thermal shock in an effective manner. Gürcan and Yakar (2022) analyzed the power output of a TEG located in a turbocharged tractor between the compressor and intercooler. They emphasized that this system's power output could be employed for electrically powered devices, such as a TEC refrigerator, the electrical power need of which could be met through the use of the TEG system. Gürcan and Yakar (2022) examined the impact of widths of thermocouples on the conversion from thermal to electric energy. According to their results, the increase in current was 14.67% at = 0.75; 15.4% at = 1; 15.95% at = 1.25, and 16.2% at = 1.5 for the TGM-199-1.6-2.0, when compared to the TGM-199-1.4-2.0.

The aim of the present study is to optimize a TEC for a turbocharged tractor. Moreover, the electrical energy need of this TEC is supplied by a TEG system that obtains power by using the air leaving the compressor of the turbocharged tractor (the literature generally discusses TEG systems that use the exhaust gas). Thanks to the TEC powered by this TEG system, farmers working in the field for long periods of time will be able to preserve the food and the cold beverages they need easily, especially in summer. In addition, the power requirement of this system is supplied by the TEG system on the same tractor, so it is possible to operate the mini refrigerator without additional fuel consumption. This means that the tractor owner can achieve these comfort conditions at no additional cost.

When the literature is examined, no study has been found in which cooling is done by using the compressor air of turbocharged systems. However, this work uses the compressor air to cool the refrigerator. This is the innovative aspect of the work.

2. Design of Mini Refrigerator With TEC

The mini refrigerator with TEC was designed to fit inside a turbocharged tractor (Arıcıoğlu, 2021). It was planned that the refrigerator door would open from above in order to save the volume inside the tractor (Figure 1). The electrical energy need of this TEC was supplied by a TEG system that could obtain electrical power using the air leaving the compressor of the turbocharged tractor (Gürcan, 2019). In the literature TEG systems generally use the exhaust gas. Thanks to this TEC mini refrigerator powered by the TEG system, farmers will be able to preserve their food and cool their drinks during working hours, especially in summer, without any additional fuel consumption.

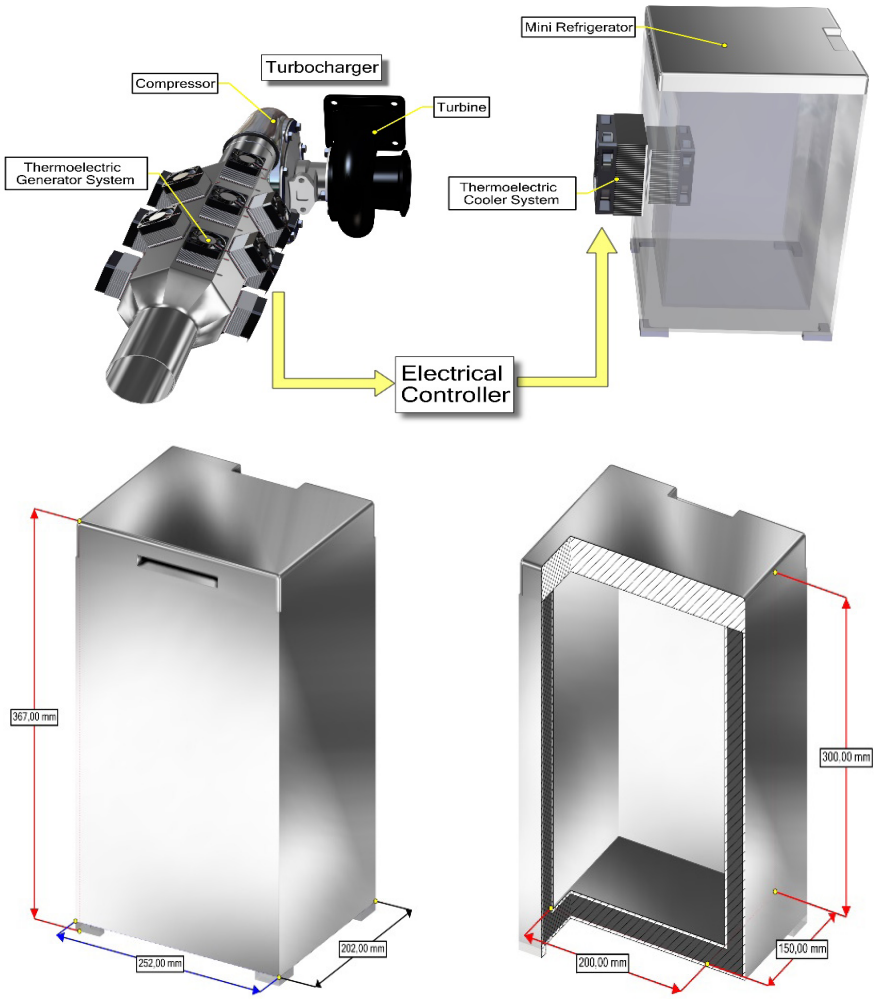

Figure 1. (a) The Mini Refrigerator with TEC Powered by TEG (b) External View and Dimensions (c) Internal Volume and Dimensions

30 mm thick polyurethane foam insulation material was used on the upper surface, while a 20 mm thick layer of the same material was used on all other surfaces of the mini refrigerator. Thus, the amount of heat gain from the warmer outdoor environment was reduced. In addition, 3 mm thick Acrylonitrile Butadiene Styrene plastic material was used to cover the interior and exterior of this refrigerator. The interior volume of the refrigerator was designed to be 9 liters and the internal volume was kept at a constant temperature of 5°C. A TB-127-1.0-1.3 commercial TEC module was used in the mini refrigerator; where TB – TE battery; 127 – number of thermocouples; 1.0 – width of thermoelement, mm;

1.3 – leg length of thermoelement, mm. To detect how seasonal temperatures affected the numerical conclusions of this present work, analyses were performed with regard to specific outdoor temperatures (15, 20, 25, 30, 35, 40 and 45 °C).

Figure 2 shows a single thermocouple (a) and a TEC with two finned surfaces (b). In addition, Figure 3 provides an illustration of three-dimensional model of the TEC module.

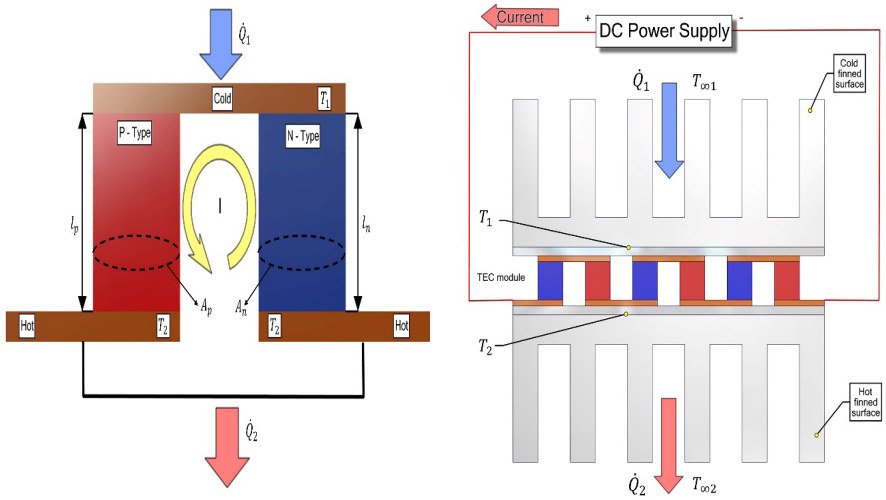

Figure 2. (a) A Thermocouple for a TEC (b) A TEC Module with Two Finned Surfaces

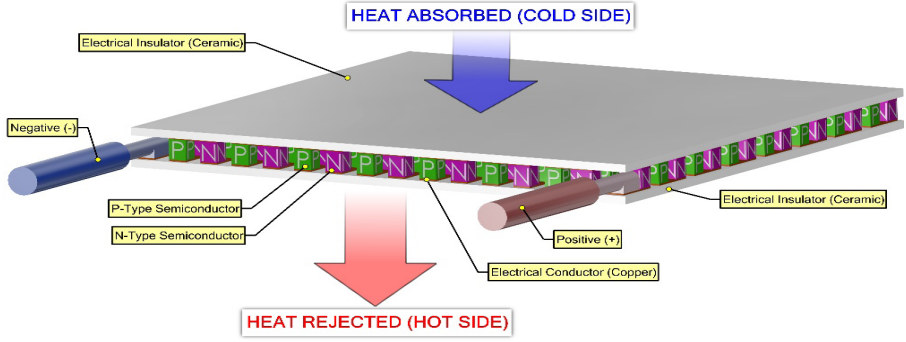

Figure 3. A TEC Module

As seen Figure 2b, when a DC voltage is applied to the TEC module or power is consumed, due to the properties of the thermocouple materials inside the mod-

ule -heat is drawn onto one surface of the module and cooling occurs depending on the direction and magnitude of the applied voltage.

A TE module is formed of series of thermocouples that consists of p-type and n-type thermoelements. Furthermore, these thermocouples are electrically connected in series and thermally connected in parallel. The thermoelement's leg length and cross-sectional area were and respectively. There were 127 thermocouples.

Research and publication ethics were complied with in this study.

3. Mathematical Expression of a TEC

The effective rejection or absorption of thermal energy through the use extended surfaces, such as fins is important. TEC modules largely deploy finned structures (heat sinks) for this reason. In the present study, the heat sink shown in Figure 4 was used.

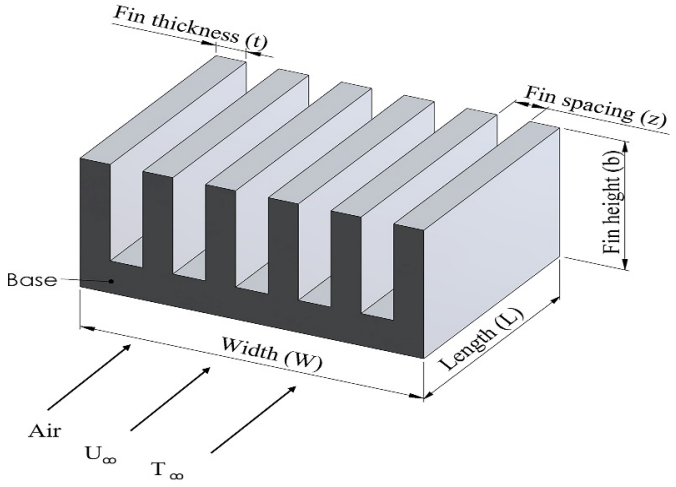

Figure 4. The Heat Sink Used This Study

The volume of the heat sink is fixed (Figure 4). For this reason, it is important to detect the optimum fin thickness (Lee, 2010). The fins used in the study were made of aluminum. The number of fins used in this study:

$$n_f = \frac{W}{z_{opt}+t} \tag{1}$$

where w is the finned structure width. In this equation, fin thickness is denoted

by t and optimum fin spacing is denoted by $_{zopt}$.

Equation (2) shows the fin efficiency:

$$\eta_f = \frac{tanh(\beta)}{\beta} \tag{2}$$

where

$$\beta = b\left(\frac{2h}{k_{al}t}\right) \tag{3}$$

where fin height is denoted as b, h represents the heat convective coefficient, and the thermal conductivity of the fin material is denoted by $_{kal}$.

A_f is the area of the fin:

$$A_f = 2\ (L+t)\ b \tag{4}$$

A_t is the sum finned surface area:

$$A_t = n_f\ (A_f + Lz_{opt}) \tag{5}$$

where the length of the finned structure is denoted as L. η is the efficiency of the overall finned surface:

$$\eta = 1 - n_f \frac{A_f}{A_t}\left(1 - \eta_f\right) \tag{6}$$

$\dot{Q}_t$ is the sum heat transfer rate:

$$\dot{Q}_t = \eta A_t h\ (T_{Base} - T_\infty) \tag{7}$$

where the finned structure base temperature is shown as T_{Base}, and the air temperature is denoted as T_∞.

The optimum fin spacing (z_{opt}) is written as follows (Lee, 2010):

$$z_{opt} = L_c 3.24 Re^{-1/2} Pr^{-1/4} \tag{8}$$

where the Reynolds number represents $Re\ (Re = \frac{U_\infty L_c}{\nu})$, Pr indicates the Prandtl number, the kinematic viscosity is denoted as ν, L_c, shows the characteristic length of flow, and U_∞ represents the velocity of air flow.

$$h = \frac{k_{air}}{L_c} 0.664 Re^{1/2} Pr^{1/3} \tag{9}$$

where the thermal conductivity of air is shown by k_{air}.

The MATLAB^R software was used with Equations (1) to (9) inclusive to determine the productivity of the finned structure for every thickness of fin, as well as to establish the optimum thickness of fin. Figure 5 illustrates the flow chart for the optimal values.

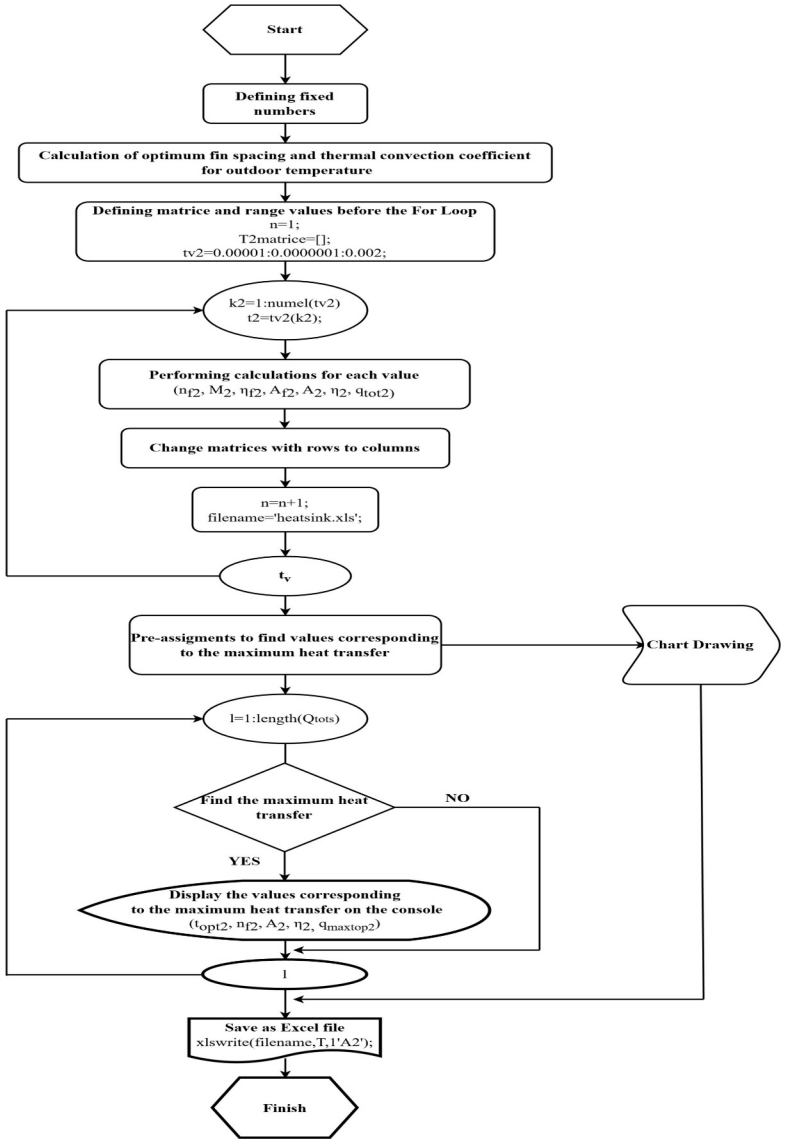

Figure 5. MATLAB^R Flow Chart for Optimal Values of Finned Structure on Hot Surface

The TE properties of the modules are not temperature dependent (Lee, 2017).

Numerical analyses were performed using the basic equations. These equations were formulated as following:

$\dot{Q}_1$ is the rate of heat absorbed at the cold side:

$$\dot{Q}_1 = n\left[\alpha I T_1 - \frac{1}{2} I^2 R - K(T_2 - T_1)\right] \tag{10}$$

$$\dot{Q}_1 = \eta_1 h_1 A_{t1}(T_{\infty 1} - T_1) \tag{11}$$

$\dot{Q}_2$ is the rate of heat liberated at the hot side:

$$\dot{Q}_2 = n\left[\alpha I T_2 + \frac{1}{2} I^2 R - K(T_2 - T_1)\right] \tag{12}$$

$$\dot{Q}_2 = \eta_2 h_2 A_{t2}(T_2 - T_{\infty 2}) \tag{13}$$

where the number of thermocouples of the module is shown by n, the cold surface temperature of the TEC module is denoted as T_1, the hot surface temperature of TEC module is shown as T_2, the cold ambient temperature is shown by $T_{\infty 1}$, the outdoor temperature is denoted by $T_{\infty 2}$ and electrical current is shown as I. Also, α, R, , and K are defined as follows, respectively:

$$\alpha = \alpha_p - \alpha_n \tag{14}$$

$$R = \frac{\rho_p l_p}{A_p} + \frac{\rho_n l_n}{A_n} \tag{15}$$

$$K = \frac{k_p A_p}{l_p} + \frac{k_n A_n}{l_n} \tag{16}$$

The internal electrical resistance is denoted by R and K indicates the thermal conductance. It is $R = \rho l/A$ and $K = kA/l$, $\rho = \rho_p + \rho_n$ and $k = k_p + k_n$. Moreover, shows the Seebeck coefficient, the thermal conductivity is shown by k, the electrical resistivity is denoted by , the leg length of the thermocouples is shown by l and the cross-sectional area of the thermocouples is shown as A (Lee, 2017).

According to $\dot{W} = \dot{Q}_2 - \dot{Q}_1$, power input required for the TEC can be defined as follows:

$$\dot{W} = n[\alpha I(T_2 - T_1) + I^2 R] \tag{17}$$

Since the electrical power input is $\dot{W} = IV$, the voltage across the TEC module can be defined as

$$V = n[\alpha(T_2 - T_1) + IR] \tag{18}$$

The coefficient of performance is written by

$$COP = \frac{\dot{Q}_1}{\dot{W}} = \frac{n\left[\alpha T_1 I - \frac{1}{2} I^2 R - K(T_2 - T_1)\right]}{n[\alpha I(T_2 - T_1) + I^2 R]} \tag{19}$$

The study aimed to simulate how the TEC module would perform by employing these ideal Equations (10) to (19). TEC producers provide maximum parameter values $(I_{max}, V_{max}, \dot{Q}_{max} \text{ and } \Delta T_{max})$ (and) in their catalogs of products. However, the α, and k are not provided. Lee (2017) thus detailed the effective material properties. These properties need to be halved because TE material properties contain both thermoelements. indicates the effective figure of merit:

$$Z^* = \frac{2\Delta T_{max}}{(T_2 - \Delta T_{max})^2} \tag{20}$$

The effective Seebeck coefficient:

$$\alpha^* = \frac{2\dot{Q}_{1max}}{nI_{max}(T_2 + \Delta T_{max})} \tag{21}$$

The effective electrical resistivity is:

$$\rho^* = \frac{\alpha^*(T_2 - \Delta T_{max})A/l}{I_{max}} \tag{22}$$

The effective thermal conductivity:

$$k^* = \frac{(\alpha^*)^2}{\rho^* Z^*} \tag{23}$$

Novel dimensionless groups have been determined to represent the significant parameters of TECs. It is necessary, in particular, to use the convection conductance of a fluid in the denominators of the dimensionless parameters. Thus, the determination of the optimum thermoelements number or optimal thermal conductance is provided (Lee, 2017).

N_k is the dimensionless thermal conductance:

$$N_k = \frac{n(Ak/l)}{\eta_2 h_2 A_{t2}} \tag{24}$$

N_h is the dimensionless convection:

$$N_h = \frac{\eta_1 h_1 A_{t1}}{\eta_2 h_2 A_{t2}} \tag{25}$$

NI is the dimensionless current:

$$N_I = \frac{\alpha I}{Ak/l} \tag{26}$$

The dimensionless temperatures can be defined by

$$T_1^* = \frac{T_1}{T_{\infty 2}} \tag{27}$$

$$T_2^* = \frac{T_2}{T_{\infty 2}} \tag{28}$$

$$T_\infty^* = \frac{T_{\infty 1}}{T_{\infty 2}} \tag{29}$$

The dimensionless cooling power is:

$$Q_1^* = \frac{\dot{Q}_1}{\eta_2 h_2 A_{t2} T_{\infty 2}} \tag{30}$$

The dimensionless rate of heat liberated is:

$$Q_2^* = \frac{\dot{Q}_2}{\eta_2 h_2 A_{t2} T_{\infty 2}} \tag{31}$$

*W** is the dimensionless electrical power input:

$$W^* = \frac{\dot{W}}{\eta_2 h_2 A_{t2} T_{\infty 2}} \tag{32}$$

Utilizing the novel dimensionless groups expressed in Equations (24) through (29), Equations (10) through (13) reduce to two correlations:

$$\frac{N_h (T_\infty^* - T_1^*)}{N_k} = N_I T_1^* - \frac{(N_I)^2}{2ZT_{\infty 2}} + (T_1^* - T_2^*) \tag{33}$$

$$\frac{T_2^* - 1}{N_k} = N_I T_2^* + \frac{(N_I)^2}{2ZT_{\infty 2}} + (T_1^* - T_2^*) \tag{34}$$

where $Z=\alpha^2/\rho k$ (the figure of merit). Equations (33) and (34) can be solved for T_1^* and T_2^*. Dimensionless temperatures depend on five independent dimensionless parameters:

$$T_1^* = f(N_k, N_h, N_I, T_\infty^*, ZT_{\infty 2}) \tag{35}$$

$$T_2^* = f(N_k, N_h, N_I, T_\infty^*, ZT_{\infty 2}) \tag{36}$$

T_∞^* is the input and $ZT_{\infty 2}$ is the material property with the input. Both of these are given in the first instance. It is thus only possible to conduct optimization using, N_k , N_h and N_I parameters. After T_1^* and T_2^* have been calculated, the dimensionless heat transfer rates are found:

$$Q_1^* = N_h(T_\infty^* - T_1^*) \tag{37}$$

$$Q_2^* = T_2^* - 1 \tag{38}$$

Then, the dimensionless power input can be given by

$$W^* = Q_2^* - Q_1^* \tag{39}$$

Accordingly, the coefficient of performance can be written as

$$COP = \frac{Q_1^*}{W^*} \tag{40}$$

the dimensionless voltage is defined as

$$N_V = \frac{V}{n\alpha T_{\infty 2}} \tag{41}$$

and, dimensionless voltage is obtained by

$$N_V = \frac{W^*}{N_I N_k} \tag{42}$$

Placing the values calculated in Equations (33) and (34) leads to the formation of two equations with four unknowns. If T_1^* and T_2^* are to be determined on the basis of these equations, values must be known for N_I and N_k. These are thus entered as incremental values in the MATLAB^R. Optimum values were determined according to maximum cooling power. In this manner, T_1^*, T_2^* were obtained. Figure 6 presents the flow chart in relation to values obtained for the maximum cooling power, while Figure 7 presents the flow chart with regard to the optimization of these values for the optimum design. Table 1 shows the dimensionless values from the analysis using the MATLAB^R program for the seven specific outdoor temperatures according to the flow charts in Figures 6 and 7.

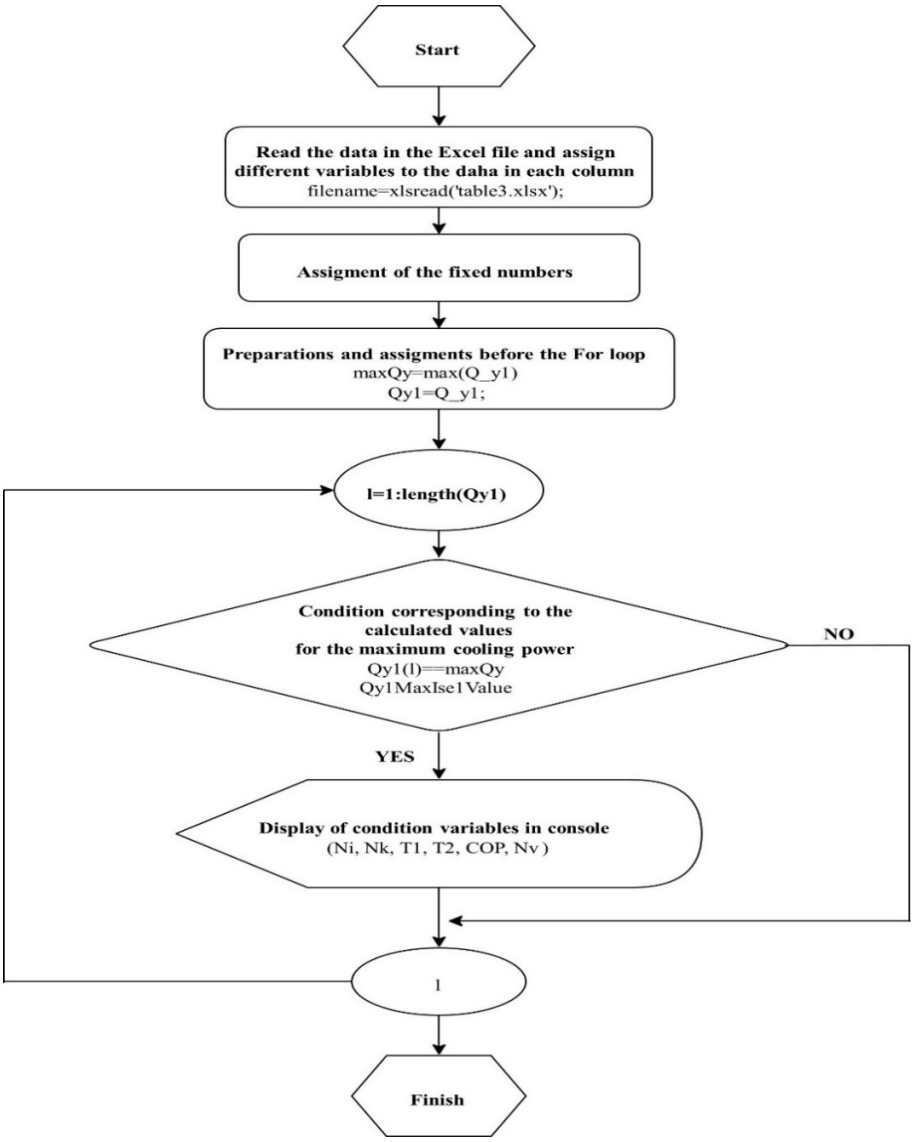

Figure 6. MATLAB[R] Flow Chart in Relation to Values Obtained for Maximum Cooling Power

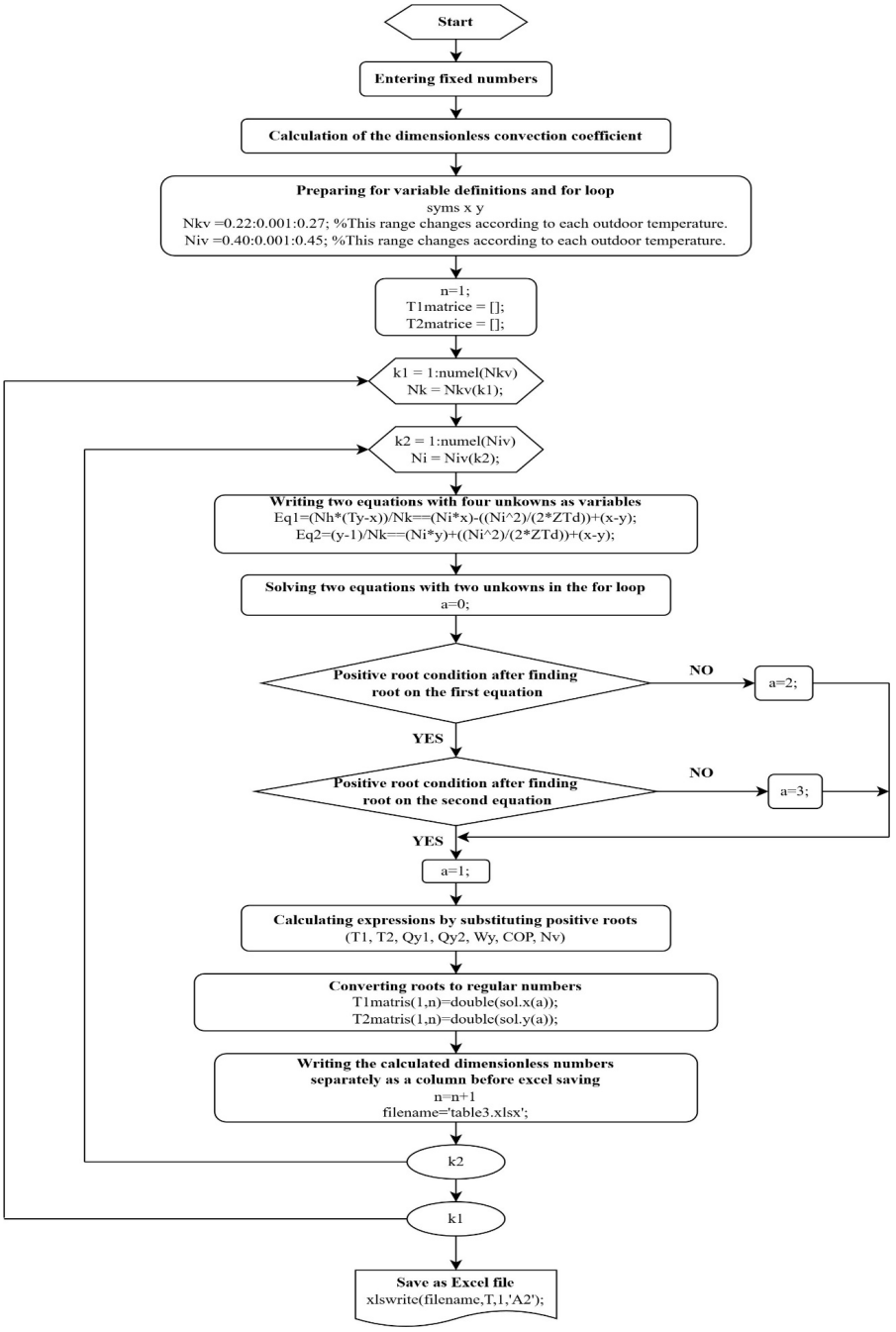

Figure 7. MATLAB[R] Flow Chart with regard to Solution of Optimization Values

Table 1. Optimal Dimensionless Parameters for the TB-127-1.0-1.3

$T_{\infty 2}$ (K)	T_{∞}^{*}	T_1^*	T_2^*	N_h	N_k	N_I	N_v	Q_1^*	COP
318	0.874	0.858	1.073	0.642	0.145	0.522	0.843	0.0099	0.156
313	0.888	0.869	1.079	0.635	0.162	0.503	0.824	0.0118	0.176
308	0.902	0.880	1.084	0.626	0.180	0.485	0.806	0.0138	0.197
303	0.917	0.891	1.089	0.618	0.199	0.467	0.787	0.0160	0.219
298	0.932	0.902	1.094	0.609	0.220	0.448	0.766	0.0184	0.244
293	0.948	0.913	1.098	0.599	0.243	0.429	0.745	0.0210	0.271
288	0.965	0.925	1.103	0.593	0.269	0.409	0.721	0.0239	0.301

4. Validation of the Numerical Solution

In order to verify the numerical solution, the performance values found by way of the use of the MATLAB^{R} software for the TB-127-1.0-1.3 were compared with the performance values informed in the company catalog (Kryotherm, 2018). Table 2 compares the performance values found by the company through experimentation with the performance values obtained with the MATLAB^{R} software.

Table 2. Verification of the Numerical Solution

Performance values	I (A)	ΔT (K)	$\dot{Q}_1$ (W)	V (V)
Company catalog (Experimentally)	3.6	69	34.5	15.7
Present study (Numerically)	3.6401	68.31	34.082	15.567
Relative error	1.11%	0.99%	1.21%	0.84%

The numerical conclusions of the present study were in accord with the conclusions obtained through experimentation in the company catalogue (Table 2).

5. The Numerical Analysis Results

In this study, a TEC mini refrigerator was designed to fit inside a turbocharged tractor. The electrical energy need of this TEC was supplied by a TEG system that could generate electrical power by utilizing the air compressed by the tractor's compressor. Thanks to this mini refrigeration with a TEC working with a TEG system, farmers will be able to preserve their food and cool their drinks during working hours, especially in summer, without any additional fuel consumption. Analyses were carried out for the seven specific outdoor temperatures to detect what effect different summer and winter conditions would have. The analysis

results using the MATLAB[R] software were found for a single TB-127-1.0-1.3. However, as the outdoor temperature increased, a single TEC module was not sufficient at outdoor temperatures above approximately 30 °C, as seen in Figure 12, and two TEC modules were needed.

5.1 Results Concerning Performance Analysis

Figure 8 shows the alterations in the cooling power and the coefficient of performance for seven different outdoor temperatures.

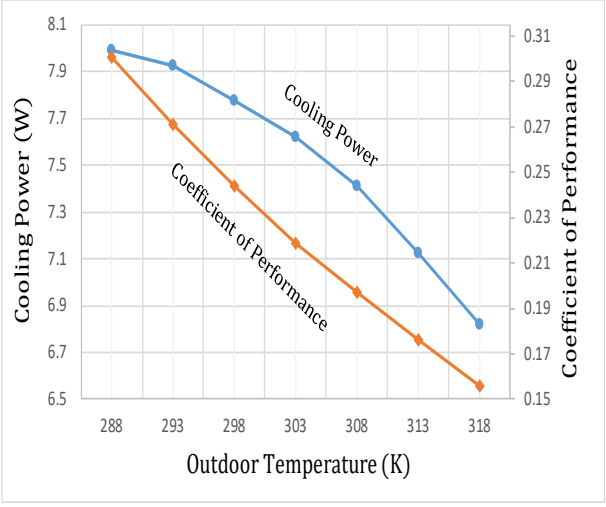

Figure 8. Variation of Cooling Power and Coefficient of Performance of TEC Module with Different Outdoor Temperatures

The cooling power decreased with increasing outdoor temperature (Figure 8). This is because as the outdoor temperature increases, the temperature difference between hot and cold surfaces increases. In other words, the maximum cooling power in TECs is obtained at = 0 K (Lee, 2017). In addition, the surface temperature of the cold side increased with an increment in the outdoor temperature. This means less heat is absorbed from the volume to be cooled at the constant cold ambient temperature. As a result, for a single TEC module, the highest cooling power was obtained as 7.989 W at 288 K outdoor temperature and the lowest cooling power was 6.818 W at 318 K outdoor temperature.

Figure 8 shows that the coefficient of performance also decreased with increasing outdoor temperatures. This situation is observed in all cooling systems. The same is also openly seen in the coefficient of performance of the reversed Carnot cycle. Accordingly, it was determined that the maximum coefficient of perfor-

mance value was 0.301 at 288 K outdoor temperature and the lowest coefficient of performance value was 0.156 at 318 K (Figure 8).

Figure 9 illustrates voltage and power input values at different current values.

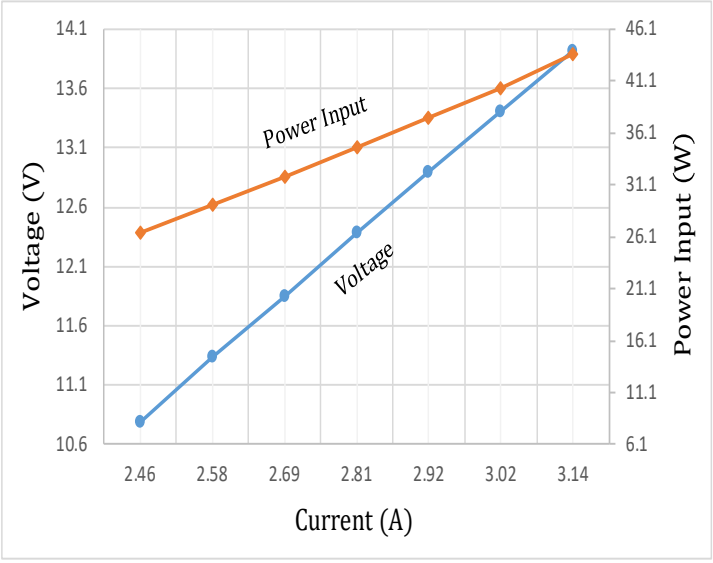

Figure 9. Voltage and Power Input for the TEC Module at Different Electrical Current

As seen in Figure 9, The voltage and the power input also increased with the electrical current. That is, the voltage and the power input were increased with the outdoor temperature. It was observed that the slope of the voltage curve was steeper than the slope of the power input curve. In addition, both voltage and power input curves showed a linear behavior (Figure 9). The highest power input required was around 43.70 W, and the highest voltage was 13.92 V.

Figure 10 shows the variation of the power input and the coefficient of performance with different outdoor temperatures.

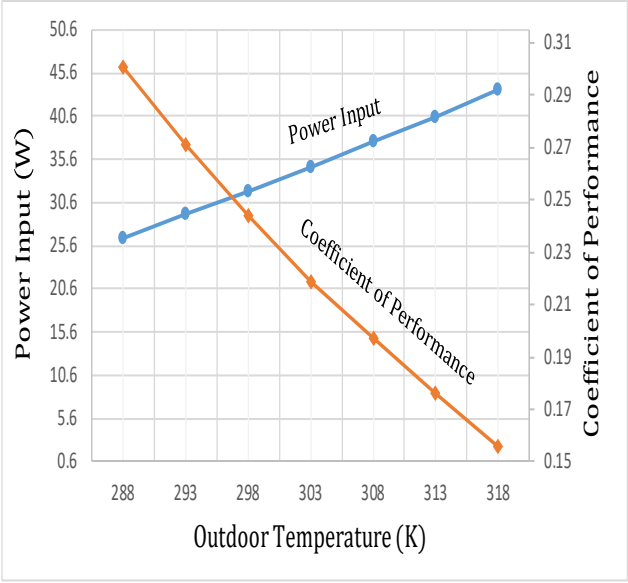

Figure 10. Power Input and Coefficient of Performance of the TEC Module at Different Outdoor Temperatures

As the outdoor temperature increased, the amount of heat gain of the volume desired to be cooled increased (Figure 10). Therefore, the cooling power absorbed by the module decreased. In this case, the required electrical energy increased as the outdoor temperature increased. As a result, the TEC required further electrical energy in summer months. Moreover, Figure 10 shows that the variation of the power input and the coefficient of performance at different outdoor temperatures was inversely proportional to each other. That is, an increasing outdoor temperature was accompanied by an increasing power input of the TEC module, but the coefficient of performance decreased. This is an expected result for the refrigeration cycle.

Figure 11 shows the variation in current and voltage for different outdoor temperatures.

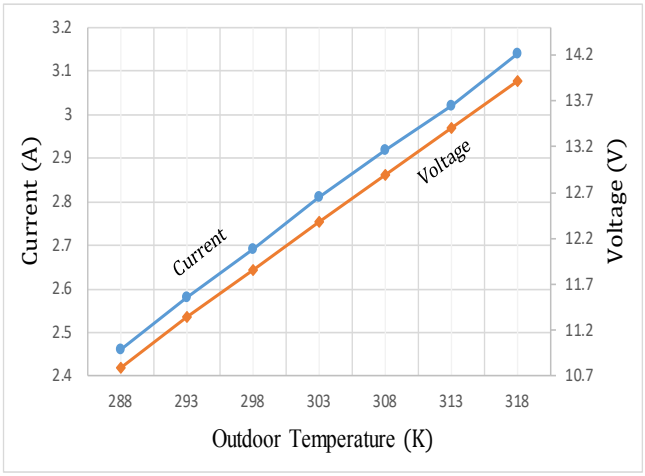

Figure 11. Current and Voltage for the TEC Module at Seven Different Outdoor Temperatures

As shown in Figure 11, the current required of the module increased with increasing outdoor temperature. This was because, as the outdoor temperature increased, the heat gain of the environment to be cooled increased. In TE cooling systems, it is known that the medium that carries the heat from the cold environment to the warm environment is the current. Therefore, as the outdoor temperature increases, the current circulating in the system is expected to increase. As a result, it was determined that the maximum current value was 3.14 A at 318 K outdoor temperature and the minimum current value was 2.46 A at 288 K (Figure 11).

As seen in Figure 11, as the outdoor temperature increased, so the voltage also had a tendency to increase. This behavior is expected in TECs. An increase in power input and current in the TEC module signifies an increase in voltage. In summary, an increase was required in the electromotive forces in these conditions. Accordingly, the maximum voltage was 13.92 V at 318 K while the minimum voltage was 10.79 V at 288 K.

Figure 12 illustrates the change in the number of TEC modules according to different outdoor temperatures.

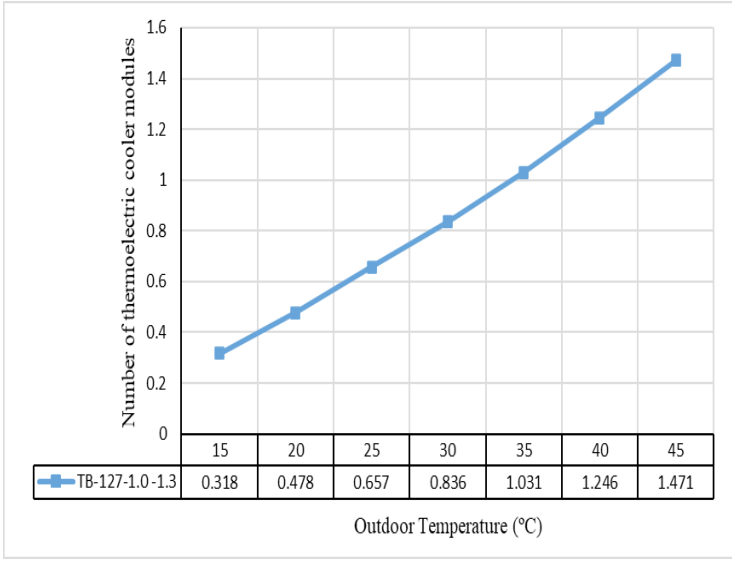

Figure 12. Number of the TEC Modules for Different Outdoor Temperatures

As the outdoor temperature increased, the number of TEC modules that required to be used in the mini refrigerator increased (Figure 12). The number of TEC modules was more than one at outdoor temperatures above about 30 °C. In other words, a single TEC module was insufficient for outdoor temperatures above approximately 30 °C, and two TEC modules were required.

5.2 Results Concerning Dimensionless Parameters

In this section, the changes in Q_1^*, W^*, COP, T_1^* and T_2^* and according to the incrementally entered and values of the optimized TB-127-1.0-1.3 are shown in Figure 13a–c, respectively.

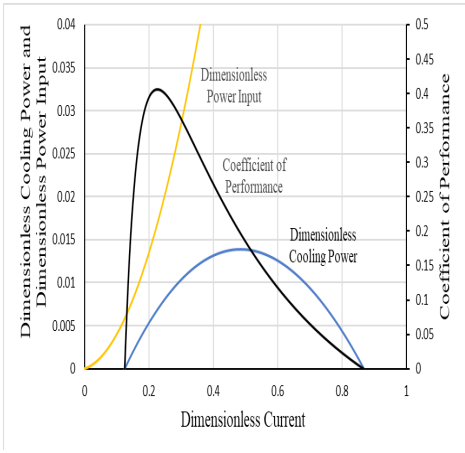

(a)

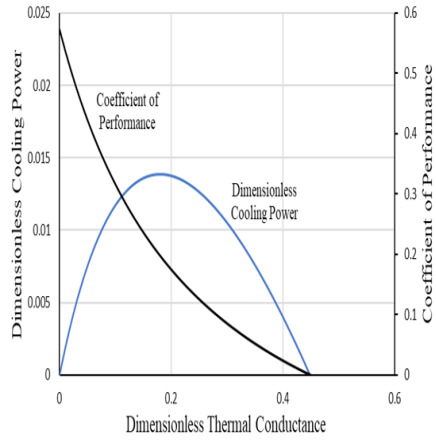

(b)

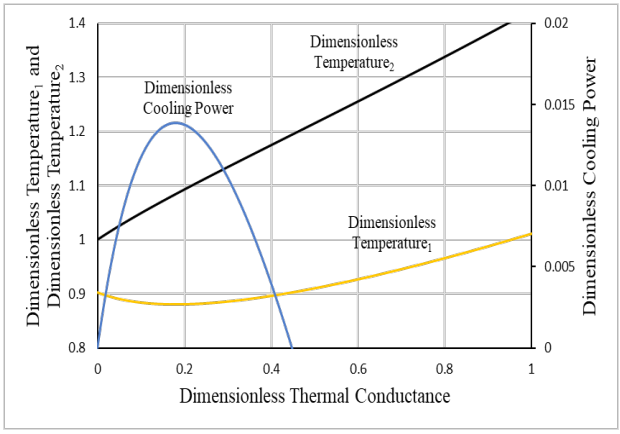

(c)

Figure 13. (a) Change of Dimensionless Cooling Power, Power Input, and Coefficient of Performance according to Dimensionless Current (b) Change of Dimensionless Cooling Power and Coefficient of Performance with Dimensionless Thermal Conductance (c) Effect of Dimensionless Thermal Conductance on Dimensionless Temperatures and Dimensionless Cooling Power

These graphs were created according to the optimum values N_k = 0.18, N_l = 0.485, N_h = 0.626, T_∞^* = 0.902 and $ZT_{\infty 2}$ = 0.805 for outdoor temperature $T_{\infty 2}$ = 35°C. *It can be seen that the optimum design parameter curves in Figure 13 and the optimum design parameter curves shown in the Reference (Lee, 2017) are in agreement.* For the outdoor temperature of 35 °C, it was observed that with the increase of the dimensionless current (N_l), there was no cooling up to 0.137 of the

(N_I), and the cooling started when the value reached 0.137 (Figure 13a). This may be due to the fact that the electrical power consumed by the module was not sufficient for the required cooling power until it reached N_I = 0.137. It can also be seen in Figure 13a that the value of dimensionless cooling power is not the maximum at the maximum coefficient of performance value. This is an expected result in TEC modules. This is because, as seen in Figure 13a, it is known that the cooling power is ineffective at the point where the coefficient of performance value is at the maximum and in some cases it is almost negligible (Lee, 2017). In addition, the maximum coefficient of performance value was obtained when the dimensionless power input and dimensionless cooling power curves were closest to each other (Figure 13a).

In TECs, it is known that the optimum cooling power is a function of the current. However, there is no information in the literature that there is an optimal dimensionless thermal conductance (N_k) value in TE cooling systems (Lee, 2017). As seen in Figure 13b, when the value is higher than 0.48, the cooling power reaches zero. That is, when N_k is greater than 0.48, there is no cooling.

It is known that the lowest dimensionless temperature T_1^* value occurs not at the highest coefficient of performance, but at the highest dimensionless cooling power (Lee, 2017). Figure 13c also shows that, at the point where T_1^* value is minimum, dimensionless cooling power reaches its maximum value. In addition, for a specific outdoor temperature, the surface temperature of the cold side of the TEC takes the lowest value at the minimum value of T_1^* . This situation can be easily seen in Equation (27). In this case, considering that the $T_{\infty 1}$ (the cold ambient temperature) value is always constant and 5 °C, it can be concluded that the maximum heat is absorbed when the cold surface temperature is at a minimum.

5.3 Results Concerning Variation of the Performance of the TB-127-1.0-1.3 with Fin Thickness and Spacing

Figure 14 illustrates the change of the performance of the TB-127-1.0-1.3 with the fin thickness.

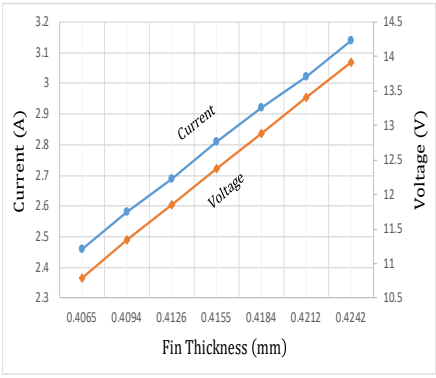

(a)

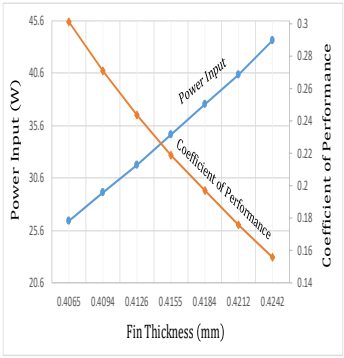

(b)

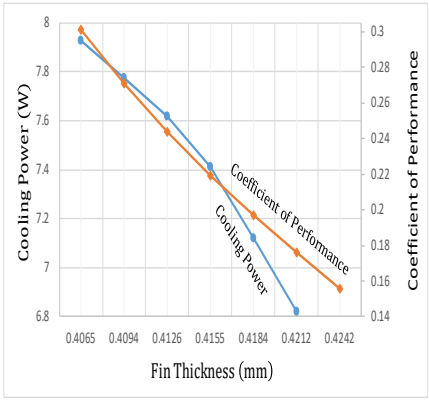

(c)

Figure 14. Effect of the Fin Thickness on Performance of TEC Module: (a) Current and Voltage (b) Power Input and Coefficient of Performance (c) Cooling Power and Coefficient of Performance

Current, voltage and power input increased with an increasing fin thickness, but cooling power and coefficient of performance decreased (Figure 14). That is, as the fin thickness increased, the temperature difference (ΔT) between the cold (T_1) and hot (T_2) surface of the module increased. Therefore, the cooling power absorbed by the module decreased. In addition, a linear behavior was observed in the changes of current, voltage, power input and coefficient of performance with fin thickness. However, this linear behavior was not observed for cooling power. The change of cooling power with fin thickness was slower up to 0.4155 mm fin thickness, and quicker after 0.4155 mm fin thickness.

The change of the performance of the TEC module with the fin spacing is also illustrated in Figure 15.

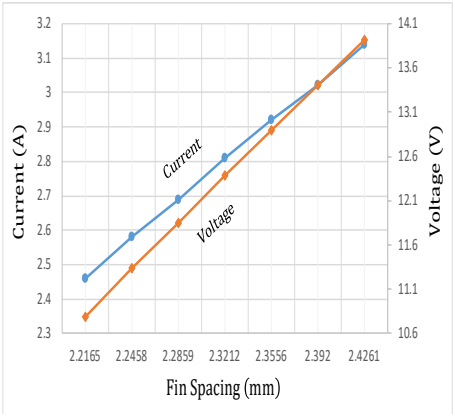

(a)

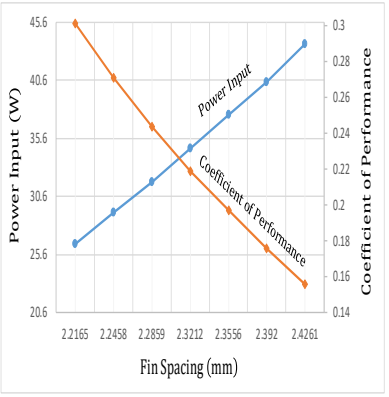

(b)

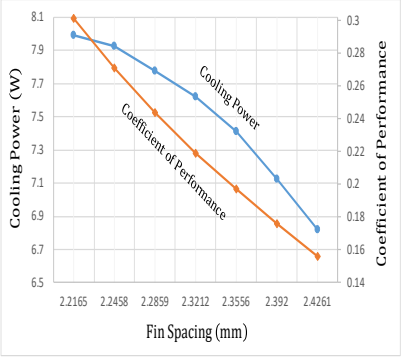

(c)

Figure 15. Effect of the Fin Spacing on Performance of TEC Module: (a) Current and Voltage (b) Power Input and Coefficient of Performance (c) Cooling Power and Coefficient of Performance

As with the fin thickness, the current, voltage and power input increased with the increasing fin spacing, but the cooling power and performance coefficient decreased (Figure 15). In other words, the productivity of the TEC decreased with increasing fin thickness and spacing. This is because, as the fin thickness and spacing increased, the temperature difference between the cold and hot sur-

face of the module increased. In addition, a linear behavior was observed in the changes of current, voltage, power input and coefficient of performance with fin spacing. However, this linear behavior was not observed for cooling power.

5.4 Results on the TEG's Capacity to Operate the TEC in the Turbocharged Tractor

In his numerical study, Gürcan (2019) obtained electrical power from a TEG in a turbocharged tractor. For the same tractor and environmental conditions, it was determined that the power input required for the TEC, which was optimized in the present work, can be met by this TEG system. This situation is illustrated in Table 3.

Table 3. Providing the Power Input Required for the TEC Using a TEG System

(K)	Power input (W) (Present study)	Power output (W) (Gürcan, 2019)	Capacity to power (%)
288	26.54	50.71	191.07
293	29.25	46.56	159.18
298	31.87	42.62	133.73
303	34.78	38.84	111.67

The sum power output values of the TEG system illustrated in Table 3 were obtained for the 1 value of dimensionless electrical resistance.

The power input of the TEC at different outdoor temperatures can be smoothly met by the TEG system (Table 3). This means that the TEC with a TEG can be used without additional fuel consumption.

6. Conclusions

The present study performed optimization of a TEC, which was driven by a TEG system. The conclusions obtained in this numeric study are summarized below:

1) The TEC performance decreased during the summer. This is an expected result for cooling systems.
2) The maximum cooling power was obtained as 7.989 W at 288 K outdoor temperature and the minimum cooling power was 6.818 W at 318 K outdoor temperature (for a single TEC module).
3) The maximum coefficient of performance value was 0.301 at 288 K outdoor temperature and the lowest coefficient of performance value was 0.156 at 318 K.
4) The voltage and the power input increased with an increase in the electrical current.

5) The maximum current value was 3.14 A at 318 K outdoor temperature and the minimum current value was 2.46 A at 288 K.
6) With increasing outdoor temperature, the voltage increased, and the maximum voltage was 13.92 V at 318 K while the minimum voltage was 10.79 V at 288 K.
7) With increasing fin thickness and spacing, current, voltage and power input increased, but cooling power and coefficient of performance decreased.
8) The power input of the TEC at different outdoor temperatures was easily met by the TEG system.

List of Symbols

A	Cross-sectional area of thermoelements (m^2)
A_t	Sum finned surface area (m^2)
A_f	Area of the fin (m^2)
b	Fin height (m)
COP	Coefficient of performance
h	Heat convective coefficient (W/m^2K)
I	Electrical current (A)
I_{max}	Maximum electrical current (A)
k	Thermal conductivity of thermoelements (W/mK)
K	Thermal conductance (W/K)
k_{al}	Thermal conductivity of fin material (aluminum) (W/mK)
k_{air}	Thermal conductivity of air (W/mK)
k^*	Effective thermal conductivity (W/mK)
l	Leg length of thermoelements (m)
L	Length of finned structure (m)
L_c	Characteristic length of flow (m)
n	Number of thermocouples of TEC
n_f	Number of fins
N	Number of TEC modules
N_k	Dimensionless thermal conductance
N_h	Dimensionless convection
N_I	Dimensionless current
N_V	Dimensionless voltage

P_r	Prandtl number
$\dot{Q}_{1max}$	Maximum cooling power (W)
$\dot{Q}_1$	Cooling power of TEC module (W)
Q_1^*	Dimensionless rate of heat transfer on cold side
$\dot{Q}_2$	Heat liberated at the hot surface (W)
Q_2^*	Dimensionless rate of heat transfer on hot side
$\dot{Q}_t$	Sum heat transfer rate of finned structure (W)
R	Internal electrical resistance (Ω)
R_e	Reynolds number
t	Fin thickness (m)
T_1	Cold surface temperature of TEC module (K)
T_1^*	Dimensionless temperature on cold side
T_2	Hot surface temperature of TEC module (K)
T_2^*	Dimensionless temperature on hot side
$T_{\infty 1}$	Cold ambient temperature (K)
$T_{\infty 2}$	Outdoor temperature (K)
T_∞^*	Dimensionless temperature
T_{Base}	Base temperature of finned structure (K)
U_∞	Velocity of air flow (m/s)
V	Voltage (V)
V_{max}	Maximum voltage (V)
w	Width of finned structure (m)
$\dot{W}$	Power input (W)
W^*	Dimensionless power input
Z	Figure of merit (1/K)
z	Fin spacing (m)
z_{opt}	Optimum fin spacing (m)
Z^*	Effective figure of merit (1/K)

Greek symbols

α	Seebeck coefficient (V/K)
α^*	Effective Seebeck coefficient (V/K)
ΔT	Temperature difference between cold and hot surface of TEC module (K)
ΔT_{max}	Maximum temperature difference (K)

η Overall finned surface efficiency (%)

η_f Fin efficiency (%)

ν Kinematic viscosity (m^2/s)

ρ Electrical resistivity (Ωm)

ρ^* Effective electrical resistivity (Ωm)

Subscripts

1 Cold side

2 Hot side

n n-type TE element

p p-type TE element

Acknowledgements

The authors are thankful to the Pamukkale University Scientific Research Projects Council (Report No. 2018FEBE035) for providing financial support to conduct Gürcan (2019)'s Master Thesis.

Conflict of Interest

No conflict of interest is declared by the authors.

Contribution of Researchers

Author 1 carried out the necessary numerical analyses according to the purpose of the study. In addition, according to the results obtained, graphs showing the relationships between important parameters were created and interpreted by Author 1. Author2 created the design and operating conditions of the system and identified the important parameters that should be found. She also enabled the creation of graphs between important parameters and made scientific interpretations and scenarios of the resulting changes. Author 3 performed the necessary numerical analysis and determined the results regarding important parameters.

References

Attar, A., Lee, H., & Weera, S. (2015). Experimental Validation of the Optimum Design of an Automotive Air-to-Air Thermoelectric Air Conditioner (TEAC). *Journal of Electronic Materials,* 44, 2177–2185. Doi: https://doi.org/10.1007/s11664-015-3750-4

Arıcıoğlu, A. K. (2021). *The use of electric energy obtained from thermoelectric gen-*

erator in thermoelectric coolers of different sizes (M.Sc. dissertation). Department of Mechanical Engineering, Pamukkale University, Denizli, Turkey.

Cheng, Y.-H., & Lin, W.-K. (2005). Geometric optimization of thermoelectric coolers in a confined volume using genetic algorithms. *Applied Thermal Engineering,* 25, 2983–2997. Doi: https://doi.org/10.1016/j.applthermaleng.2005.03.007

Chen, L., Meng, F., & Sun, F. (2012). Effect of heat transfer on the performance of thermoelectric generator-driven thermoelectric refrigerator system. *Cryogenics,* 52, 58-65. Doi: https://doi.org/10.1016/j.cryogenics.2011.10.007

Chen, W.-H., Wang, C.-C., & Hung, C.-I. (2014). Geometric effect on cooling power and performance of an integrated thermoelectric generation-cooling system. *Energy Conversion and Management,* 87, 566–575. Doi: https://doi.org/10.1016/j.enconman.2014.07.054

Chen, W.-Y., Shi, X.-L., Zou, J., & Chen, Z.-G. (2022). Thermoelectric coolers for on-chip thermal management: Materials, design, and optimization. *Materials Science & Engineering R-Reports,* 151, 100700. Doi: https://doi.org/10.1016/j.mser.2022.100700

Feng, Y., Chen, L., Meng, F., & Sun, F. (2018). Thermodynamic Analysis of TEG-TEC Device Including Influence of Thomson Effect. *Journal of Non-Equilibrium Thermodynamics,* 43, 75–86. Doi: https://doi.org/10.1515/jnet-2017-0029

Gonzalez-Hernandez, S. (2020). Unification of optimization criteria and energetic analysis of a thermoelectric cooler and heater. *Physica A: Statistical Mechanics and Its Applications,* 555, 124700. Doi: https://doi.org/10.1016/j.physa.2020.124700

Gürcan, A., & Yakar, G. (2022). Investigation of the performance of a thermoelectric generator system utilizing the thermal energy of air compressed in a compressor. *Journal of the Korean Physical Society,* 80, 467–483. Doi: https://doi.org/10.1007/s40042-022-00425-x

Gürcan, A., & Yakar, G. (2022). Improving the performance of a thermoelectric generator system utilizing the thermal energy of air compressed in the compressor of a turbocharged tractor based on different-sized modules. *Journal of the Brazilian Society of Mechanical Sciences and Engineering,* 44, 360. Doi: https://doi.org/10.1007/s40430-022-03656-y

Gürcan, A. (2019). Recovery of exhaust heat energy using thermoelectric generators in different sizes (M.Sc. dissertation). Department of Mechanical Engineering, *Pamukkale University,* Denizli, Turkey.

Hasani, M., & Rahbar, N. (2015). Application of thermoelectric cooler as a power generator in waste heat recovery from a PEM fuel cell – An experimental study. *International Journal of Hydrogen Energy,* 40, 15040–15051. Doi: https://doi.org/10.1016/j.ijhydene.2015.09.023

Huang, Y., Chen, Z., & Ding, H. (2021). Performance optimization of a two-stage parallel thermoelectric cooler with inhomogeneous electrical conductivity. *Applied Thermal Engineering,* 192, 116696. Doi: https://doi.org/10.1016/j.applthermaleng.2021.116696

Khattab, N. M., & El Shenawy, E. T. (2006). Optimal operation of thermoelectric cooler driven by solar thermoelectric generator. *Energy Conversion and Management,* 47, 407-426. Doi: https://doi.org/10.1016/j.enconman.2005.04.011

Kishore, R. A., Nozariasbmarz, A., Poudel, B., Sanghadasa, M., & Priya, S. (2019). Ultra-high performance wearable thermoelectric coolers with less materials. *Nature Communications,* 10, 1765. Doi: https://doi.org/10.1038/s41467-019-09707-8

Kwan, T. H., Gao, D., Zhao, B., Ren, X., Hu, T., Dabwan, Y. N., & Pei, G. (2021). Integration of radiative sky cooling to the photovoltaic and thermoelectric system for improved space cooling. *Applied Thermal Engineering,* 196, 117230. Doi: https://doi.org/10.1016/j.applthermaleng.2021.117230

Kryotherm, (2018). Access address: http://kryothermtec.com/catalogs.html.

Lin, L., Zhang, Y.-F., Liu, H.-B., Meng, J.-H., Chen, W.-H., & Wang, X.-D. (2019). A new configuration design of thermoelectric cooler driven by thermoelectric generator. *Applied Thermal Engineering,* 160, 114087. Doi: https://doi.org/10.1016/j.applthermaleng.2019.114087

Lu, T., Li, Y., Zhang, J., Ning, P., & Niu, P. (2020). Cooling and Mechanical Performance Analysis of a Trapezoidal Thermoelectric Cooler with Variable Cross-Section. *Energies,* 13, 6070. Doi: https://doi.org/10.3390/en13226070

Lee, H. S. (2010). *Thermal design: heat sinks, thermoelectrics, heat pipes, compact heat exchangers, and solar cells.* Hoboken, NJ: Wiley.

Lee, H. S. (2017). *Thermoelectrics: design and materials.* Chichester: Wiley.

Meng, F. K., Chen, L. G., & Sun, F. R. (2010). Extreme working temperature differences for thermoelectric refrigerating and heat pumping devices driven by thermoelectric generator. *Journal of Energy Institute,* 83, 108-113. Doi: https://doi.org/10.1016/10.1179/014426010x12682307291506

Manikandan, S., & Kaushik, S. C. (2015). Thermodynamic studies and max-

imum power point tracking in thermoelectric generator–thermoelectric cooler combined system. *Cryogenics,* 67, 52–62. Doi: https://doi.org/10.1016/10.1016/j.cryogenics.2015.01.008

Nemati, A., Nami, H., Yari, M., & Ranjbar, F. (2018) Effect of geometry and applied currents on the exergy and exergoeconomic performance of a two-stage cascaded thermoelectric cooler. *International Journal of Refrigeration,* 85, 1–12. Doi: https://doi.org/10.1016/10.1016/j.ijrefrig.2017.09.006

Qiu, C., & Shi, W. (2020). Comprehensive modeling for optimized design of a thermoelectric cooler with non-constant cross-section: Theoretical considerations. *Applied Thermal Engineering,* 176, 115384. Doi: https://doi.org/10.1016/10.1016/j.applthermaleng.2020.115384

Sun, D., Liu, G., Shen, L., Chen, H., Yao, Y., & Jin, S. (2019). Modeling of high power light-emitting diode package integrated with micro-thermoelectric cooler under various interfacial and size effects. *Energy Conversion and Management,* 179, 81–90. Doi: https://doi.org/10.1016/j.enconman.2018.10.063

Sadighi Dizaji, H., Jafarmadar, S., Khalilarya, S., & Pourhedayat, S. (2019). A comprehensive exergy analysis of a prototype Peltier air-cooler; experimental investigation. *Renewable Energy,* 131, 308–317. Doi: https://doi.org/10.1016/j.renene.2018.07.056

Shen, L., Zhang, W., Liu, G., Tu, Z., Lu, Q., Chen, H., & Huang, Q. (2020). Performance enhancement investigation of thermoelectric cooler with segmented configuration. *Applied Thermal Engineering,* 168, 114852. Doi: https://doi.org/10.1016/j.applthermaleng.2019.114852

Sun, D., Shen, L., Niu, B., Gao, C., Zhou, P., Tang, J., … Yang, L. (2022). Active thermal management of hotspot under thermal shock based on micro-thermoelectric cooler and bi-objective optimization. *Energy Conversion and Management,* 252, 115044. Doi: https://doi.org/10.1016/j.enconman.2021.115044

Tian, X.-X., Asaadi, S., Moria, H., Kaood, A., Pourhedayat, S., & Jermsittiparsert, K. (2020). Proposing tube-bundle arrangement of tubular thermoelectric module as a novel air cooler. *Energy,* 208, 118428. Doi: https://doi.org/10.1016/j.energy.2020.118428

Zhang, H., Kong, W., Dong, F., Xu, H., Chen, B., & Ni, M. (2017). Application of cascading thermoelectric generator and cooler for waste heat recovery from solid oxide fuel cells. *Energy Conversion and Management,* 148, 1382–1390. Doi: https://doi.org/10.1016/j.enconman.2017.06.089